

The effects of the introduction of Al atom into monoclinic BiVO₄: a theoretical prediction

Shanshan Yao · Kaining Ding · Yongfan Zhang

Received: 18 May 2010/Accepted: 4 August 2010/Published online: 19 August 2010
© Springer-Verlag 2010

Abstract Using density functional theory calculation within the CASTEP code, we investigated the possible various kinds of defects in the Al: *m*BiVO₄ crystals. On the one hand, the substitution of V site with Al(_{Al-V}) was studied along with one Al substitution with an oxygen vacancy (_{Al-V} + V_O). The two defect models both induced an obvious band gap narrowing. It predicted theoretically that the redshift of absorption edge phenomenon may be measured in experiment. The most obvious difference was the appearance of a valence-band hole of the former due to the charge imbalance, while the latter has reached local charge balance. On the other hand, the substitution of Bi site with Al (_{Al-Bi}) induced an increase in the band gap, but the value is still small. This indicated that _{Al-Bi} still shows higher photocatalytic activity. Moreover, we found that *m*BiVO₄ (_{Al-Bi}) and *m*BiVO₄ (_{Al-V} + V_O) should have stronger ability of photocatalytic water splitting and H₂ evolution than those of pure *m*BiVO₄ by analyzing the density of states and band edges.

Keywords Monoclinic BiVO₄ · Al introduction · Oxygen vacancy · Electronic structure · Water splitting

1 Introduction

Owing to the fact that scheelite-type ABO₄ compounds have good prospects as heterogeneous catalysts, oxide ion conductors, and possible negative electrode materials to replace the graphite presently being used in the Li-ion

batteries. Scheelite-structured ABO₄ ternary oxides are important materials from both a theoretical and a technological point of view [1]. Bismuth vanadate (BiVO₄) is one of the most widely studied and important of the scheelite-structured ABO₄ ternary oxides.

In addition, monoclinic (distortion scheelite structure) BiVO₄ (for short, *m*BiVO₄) is one of novel semiconductor photocatalysts with narrow band [2–7]. *m*BiVO₄ has shown particular promise for water photodecomposition with the reasonable band edge [8]. However, this photocatalyst has no H₂ evolution ability due to its poor reduction potential (ca. 0.0 eV vs. NHE) [9, 10], though *m*BiVO₄ possesses a valence band edge (ca. +2.4 eV vs. NHE) with a high oxidation activity of splitting water into O₂ under visible light [11]. Therefore, it is necessary to find a feasible route for enhancing the reduction activity of splitting water into H₂.

So far, there have been many reports *m*BiVO₄ doping metal is considered to be a feasible route for enhancing the photocatalytic activity such as Fe [12], Co [13–15], Cu [16, 17], Pd [18, 19], Mn [20], Ag [21–23], Ce [24], W [25], Mo [26], V [27], Bi [28]. Moreover, recent studies show that aluminum metal is a better dopant in photocatalysts due to its stable thermal expansion coefficient and physical property [29]. Nie et al. [30] synthesized a Al/ZnO composite by using chemical co-precipitation; the UV–Vis absorption spectra showed that the Al/ZnO exhibits a redshift in the absorption edge. Shon et al. [31] studied the photocatalytic activity of Al/TiO₂ and demonstrated that it photodecomposed acetaldehyde efficiently under visible light irradiation. Li et al. [32] also reported La₂AlTaO₇ showed higher photocatalytic activity than La₃TaO₇ for hydrogen evolution from water, and the effect of Al was discussed based on density function theory (DFT) calculation. However, R. Shirley et al. [33] reported Al does not

S. Yao · K. Ding (✉) · Y. Zhang
Department of Chemistry, Fuzhou University,
Fujian, 350002 Fuzhou, People's Republic of China
e-mail: dknfzu@yahoo.com.cn

introduce band gap states but leads to an increase in the band gap in both anatase and rutile TiO_2 using density functional theory. This suggests that Al/ TiO_2 reduced the photocatalytic activity. However, the experimental study of the introduction of Al atom into monoclinic BiVO_4 to improve its photocatalytic activity has not been reported so far as we know.

In order to investigate the effect of Al atom in the Al: $m\text{BiVO}_4$ crystals, in this paper, the electronic structures of Al: $m\text{BiVO}_4$ were calculated using CASTEP code based on the density functional theory (DFT). First, the possible various defect models were simulated, and then we examined the preferred defect model. The correlation between the photocatalytic activity of splitting water and the electronic structure, and the variation of band edge was also discussed in detail.

2 Structure model and computational method

2.1 Structure models

BiVO_4 has a monoclinic distortion of scheelite structure that belongs to the space group $I2/b$, with experimental lattice parameters $a = 5.194 \text{ \AA}$, $b = 5.090 \text{ \AA}$, $c = 11.697 \text{ \AA}$ and the lattice angles $\alpha = \beta = 90.0^\circ$, $\gamma = 90.4^\circ$ [34]. The unit cell includes $(\text{BiVO}_4)_4$ structure, which is made up of distorted VO_4 tetrahedron and BiO_8 octahedron. In our calculations, three possible defect models have been considered. Model 1 is to substitute one Al atom for one Bi atom ($\text{sub}_{\text{Al-Bi}}$) in the BiVO_4 ; Model 2 is to substitute one Al atom for one V atom ($\text{sub}_{\text{Al-V}}$) in the BiVO_4 . Since the substitution of Al for V (i.e., one Al^{3+} ion replaces one V^{5+} ion) would induce a charge imbalance, the effect of oxygen vacancy should be further investigated. Thus, a Al substitution combines with an oxygen vacancy ($\text{sub}_{\text{Al-V}} + \text{Vo}$) forming defect model 3 to maintain overall charge. All these structures investigated here are shown in Fig. 1.

2.2 Computational details

All calculations were performed using DFT with the plane-wave pseudopotential (PWP) approach as implemented in the CASTEP code [35]. The generalized gradient approximation (GGA) functional by Perdew and Wang (PW91) [36, 37] was employed. The computational setup was the same as used in ref [38]. The core electrons were replaced by the ultrasoft pseudopotentials, and the valence atomic configurations were $6s^26p^3$ for Bi, $2s^22p^4$ for O, $3s^23p^63d^34s^2$ for V, $3s^23p^1$ for Al atom, all represented in a reciprocal space. As we know, the energy cutoff was one of the most important parameters that determine the accuracy and the cost of the calculation. The k -point sampling set

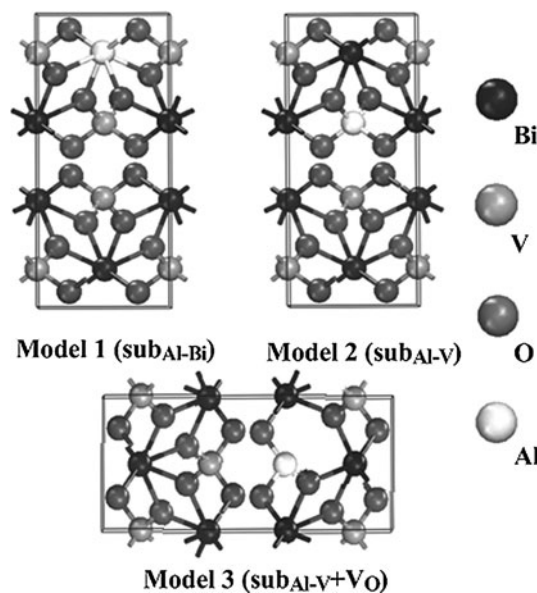


Fig. 1 The possible three defect models that are considered in this paper

defined the accuracy of the Brillouin zone. The way to determine the appropriate sets of above parameters will be discussed in the next section.

3 Results and discussion

3.1 Definition of the basis set

To gain an insight of energy cutoff required for reasonably accurate calculations, a series of test calculations were performed on the pure $m\text{BiVO}_4$ system. For these calculations, we used a k -point sampling grid of $3 \times 3 \times 1$, and both the lattice parameters and atomic positions are relaxed during the structural optimization. The relation between the energy cutoff and total energy is shown in Fig. 2. The results clearly show that the total energy is converged when the cutoff energy is larger than 500 eV. However, considering the accuracy of lattice constants [34], the energy cutoff of 340 eV is found good enough to achieve the desired convergence.

A similar test was performed to evaluate the k -point sampling required. Using the cutoff energy of 340 eV, three different k -point grids are considered. The results are shown in Fig. 2. Clearly, the size of k -point grid has small effect on the total energy which may be due to the semiconductor character of the system, so we chose an intermediate grid size of $4 \times 4 \times 2$ to study the Al: $m\text{BiVO}_4$ systems.

The results of the geometrical optimization of the pure $m\text{BiVO}_4$ at a cutoff of 340 eV and k -point sampling grid of

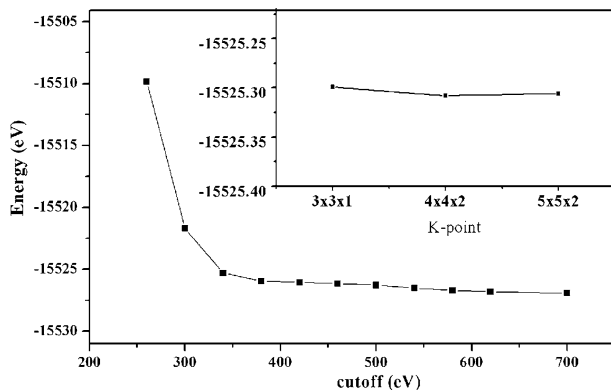


Fig. 2 The sets of cutoff energy and k -point of $m\text{BiVO}_4$ crystal

$4 \times 4 \times 2$ are given in Table 1, which are in agreement with experiment [34], with deviations of less than 1% in the lattice constants.

3.2 Structures and formation energies

A systematic study of the structural lattice parameters for $m\text{BiVO}_4$ containing impurity Al atom was carried out. From the calculation results listed in Table 1, since the ionic radius of Bi^{3+} (1.03 Å) is larger than those of Al^{3+} (0.51 Å), the $\text{sub}_{\text{Al-Bi}}$ would induce a significant local structure distortion and have a high formation energy. On the other hand, it seems that the substitution at V site results in a relative smaller lattice distortion. It is possibly because of greater difference in ionic radii between Al^{3+} and Bi^{3+} than that between Al^{3+} (0.51 Å) and V^{5+} (0.59 Å). This indicates that the substitution of Al for V requires a relatively small formation energy. We will demonstrate this by the subsequent calculated formation energy.

To study the relative stability of the possible three defect models, the defect formation energies E_{form} were calculated (Table 2). A widely accepted method for such analysis is to

evaluate their formation energies as a function of atomic chemical potentials [39]. We calculated the formation energies E_{form} according to the following equation:

$$E_{\text{form}} = E_{\text{defect}} - (E_{\text{pure}} + \mu_{\text{Al}} - \mu_{\text{M}}) \quad (1)$$

where E_{defect} and E_{pure} are the total energies of $m\text{BiVO}_4$ lattice with and without Al atom, respectively. μ_{Al} the chemical potential of impurity Al, which is obtained from the free energy of one Al atom in bulk Al. Likewise, μ_{M} is the chemical potential of the atom replaced by Al (i.e., Bi or V), which is the corresponding energy of the ground state. The calculated results are summarized in Table 2. It is noticed that the defect model is energetically more favorable while E_{form} value becomes smaller. As shown in Table 2, it can be found that the formation energy of $\text{sub}_{\text{Al-V}} + \text{V}_0$ is negative, indicating that the substitution of Al for V combining with an oxygen vacancy is most favorable. In addition, it is interesting that the formation energy of $\text{sub}_{\text{Al-Bi}}$ is lower than that of $\text{sub}_{\text{Al-V}}$, which is opposite to the situation we predicted in upper text. It is noteworthy that $\text{sub}_{\text{Al-V}}$ will generate two electron holes (which can be seen in the band structure plot) due to the charge imbalance. This is possible reason that $\text{sub}_{\text{Al-V}}$ is higher in energy. Thus, $m\text{BiVO}_4$ ($\text{sub}_{\text{Al-V}}$) is the energetically hardest to realize than the others.

3.3 Electronic structures of pure $m\text{BiVO}_4$

The band structure of the pure $m\text{BiVO}_4$ is shown in Fig. 3a. The calculated band gap between the valence band maximum (VBM) and the conduction band minimum (CBM) is about 2.21 eV, which is slightly smaller than the experimental value of 2.40 eV [5–7] due to the well-known limitation of DFT. The situation is consistent with the reports of tungstates previously [40, 41].

To analyze the origin of the electronic structure, the projected density of states (PDOS) of the pure $m\text{BiVO}_4$

Table 1 The lattice optimization for pure $m\text{BiVO}_4$ and three possible defect structures

	Exp.	Pure	$\text{Sub}_{\text{Al-Bi}}$	$\text{Sub}_{\text{Al-V}}$	$\text{Sub}_{\text{Al-V}} + \text{V}_0$
a (Å)	5.194	5.194 (0.0%)	5.124 (-1.4%)	5.139 (-1.06%)	5.164 (-0.6%)
b (Å)	5.090	5.113 (+0.5%)	5.048 (-1.3%)	5.106 (-0.14%)	5.203 (+1.8%)
c (Å)	11.697	11.753 (+0.5%)	12.024 (+2.3%)	11.634 (-1.01%)	11.779 (+0.4%)
α	90.0°	90.0°	92.4°	90.0°	90.1°
β	90.0°	90.0°	88.3°	89.9°	90.0°
γ	90.4°	90.1°	90.9°	89.8°	90.0°

Table 2 Calculated formation energies of three defect models

Model	$E_{\text{Al-doped}}$	E_{pure}	μ_{Al}	μ_{Bi}	μ_{V}	E_{form}
Model 1 $\text{sub}_{\text{Al-Bi}}$	-15432.53	-15525.30	-56.44	-147.28	-	1.93
Model 2 $\text{sub}_{\text{Al-V}}$	-13601.81	-15525.30	-56.44	-	-1977.37	2.56
Model 3 $\text{sub}_{\text{Al-V}} + \text{V}_0$	-13167.28	-15085.79	-56.44	-	-1977.37	-2.42

Unit is eV

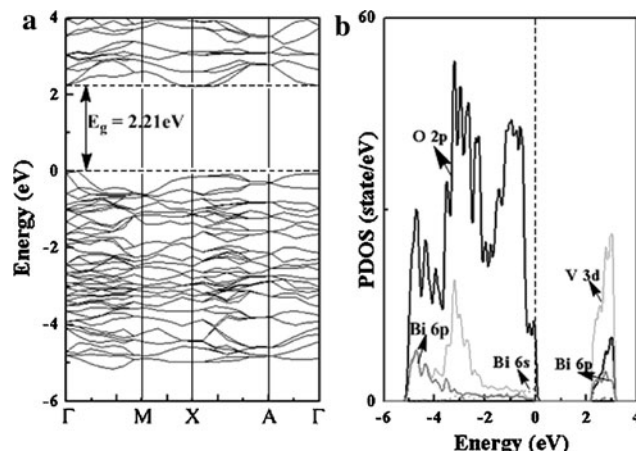


Fig. 3 The calculated electronic band structure (a) and PDOS (b) of pure $m\text{BiVO}_4$

structure is shown in Fig. 3b. It can be seen that the lower part of VBs mainly consists of O 2p orbitals and the hybridizations between O 2p and V 3d, Bi 6p are observed, implying the covalent interactions between V–O and Bi–O bonds. The upper part of VBs is dominated by O 2p orbitals with small contributions from V 3d and Bi 6s. The CBs are predominantly composed of V 3d orbitals, with significant contribution from O 2p and Bi 6p also present. An additional state is found at -9.5 eV, which is mainly consisted of the Bi 6s orbitals. Our theoretical results are consistent with those reported in previous work [8, 38].

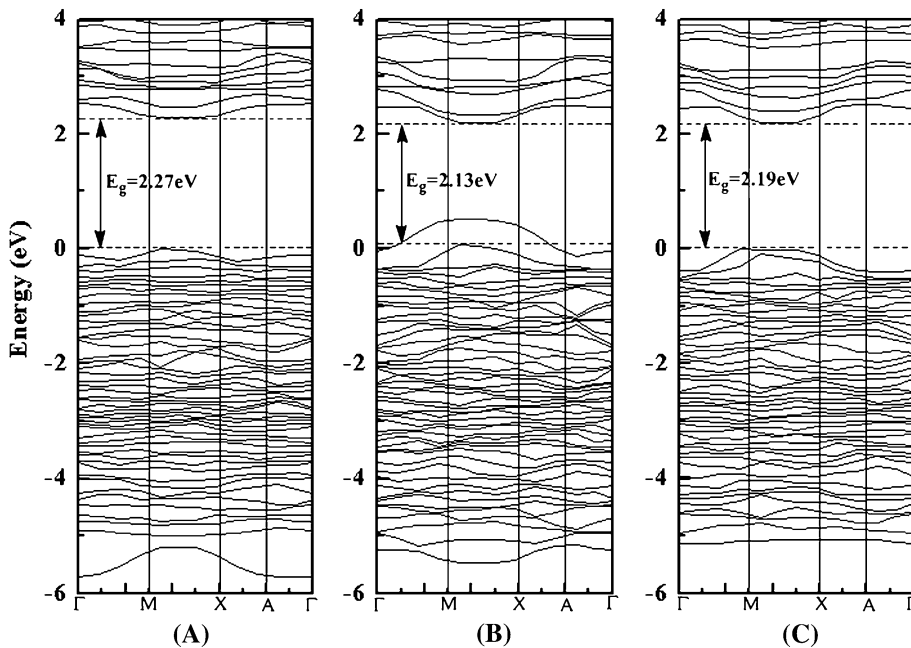
3.4 Electronic structures of defect models

3.4.1 Band structure

Figure 4 shows a comparison of the calculated energy band structure of three defect models. For model 1 ($\text{sub}_{\text{Al-Bi}}$), a new state only appears just below the bottom edge of VBs as shown in Fig. 4a. The band gap is calculated to be about 2.27 eV, which is slightly larger than the value of pure $m\text{BiVO}_4$ (2.21 eV). This suggests that visible-light photocatalytic activity is also expected. On the contrary, it is clear that a slightly decreasing of the band gap (about 0.08 eV) is observed as shown in Fig. 4b. Moreover, a valence-band hole is formed associated with charge imbalance that appears above the top of valence band. The model 2 crystal will be charged neutral, and Al requires two less electron from $m\text{BiVO}_4$ lattice. This means that 2e^- remaining per V atom replaced will have to be accommodated in the band structure.

In the case of model 3, the substitution of one V by Al combines with an oxygen vacancy leads to maintain overall charge. Figure 4c shows that the VBM and CBM of model 3 are essentially the same as those of model 2. The conduction band is expanded obviously compared with that of pure $m\text{BiVO}_4$, which results in a narrowed band gap between VBM and CBM of about 2.19 eV. This means that a redshift of absorption edge phenomenon may be observed in experiment. However, the new state is not appear above the top of VB as opposed to the situation in model 2 in which isolated states are introduced into the band gap. Our

Fig. 4 The calculated electronic band structures
a model 1 ($\text{sub}_{\text{Al-Bi}}$), b model 2
($\text{sub}_{\text{Al-V}}$) and c model 3
($\text{sub}_{\text{Al-V}} + \text{V}_\text{O}$)



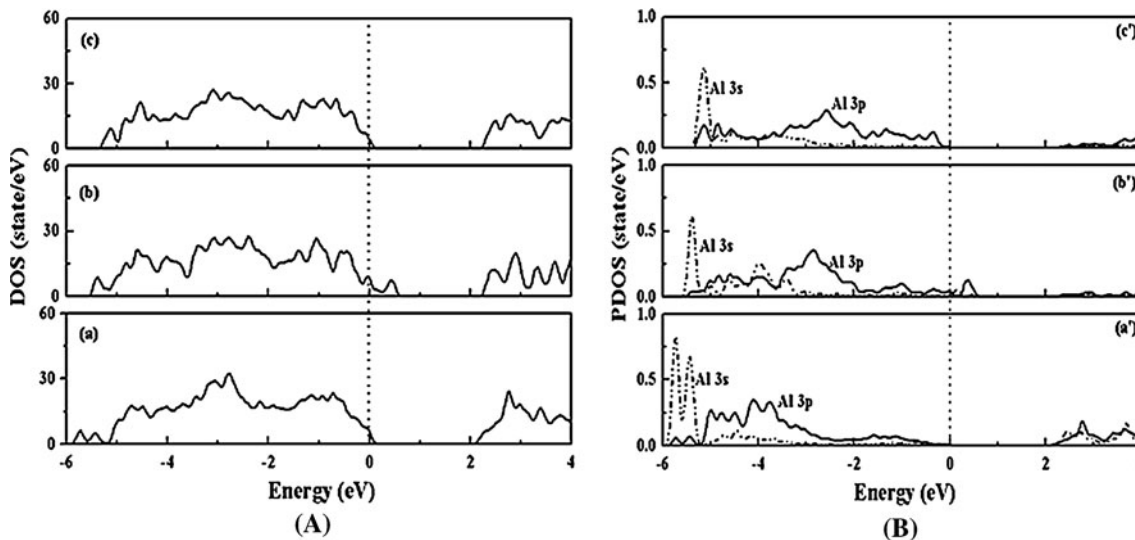


Fig. 5 The calculated TDOS of three defect models and the PDOS of Al 3s3p states (**a**, **a'**) model 1(sub_{Al-Bi}), (**b**, **b'**) model 2 (sub_{Al-V}), and (**c**, **c'**) model 3 (sub_{Al-V} + V_O)

calculations suggest this state should overlap with the top of the valence band.

3.4.2 Density of states

In order to further investigate the effect of Al 3s3p states, the TDOS of three defect models and the PDOS of Al 3s3p states were calculated and plotted in Fig. 5, panels A and B, respectively. Fermi level is regarded as the energy zero by default in these figures. Figure 5a and a' show most Al 3s3p states are located in the CBs of the model 1 structure (sub_{Al-Bi}). The mixing of Al 3s3p states with V 3d and Bi 6p states makes the position of CBM shift upwards (about 0.06 eV). Hence, it can be expected that *m*BiVO₄ (sub_{Al-Bi}) would exhibit a stronger reduction activity to split water into H₂ than pure *m*BiVO₄. This will be demonstrated in the next section about the band edge position calculation. For the model 2 structure (sub_{Al-V}), Fig. 5b and b' clearly show that the contribution of Al 3s3p states at the CBs becomes very small. Thus, the position of CBM shifts downwards slightly (about 0.02 eV), with respect to pure *m*BiVO₄. Moreover, the Al 3s3p states extend into the band gap from the VB edge of pure *m*BiVO₄ by about 0.5 eV, which is largely responsible for the band gap reduction.

But in the case of the model 3 structure (sub_{Al-V} + V_O), it is interesting that the position of the top VBs shows no significant change as well as the model 1 structure (sub_{Al-Bi}), while the position of the bottom CBs is the same as the model 2 structure (sub_{Al-V}). As a consequence, the band gap has a narrowing of about 0.02 eV when compared with that of pure *m*BiVO₄, and the ability of photocatalytic water splitting and H₂ evolution of *m*BiVO₄ (sub_{Al-V} + V_O) will be improved.

3.4.3 Band edge position calculation

For further analyzing the effect of Al substitution on the capability of photocatalysis, we also calculated the band edge position according to a semi-empirical method proposed by Butler and Ginley [42]. So far, considerable success has been achieved in calculating band position and photoelectric thresholds for many compounds using the atomic electronegativity of the constituent atoms [42–44]. The electronegativity of an atom χ defined by Mulliken is the arithmetic mean of the atomic electron affinity (A) and the first ionization energy (I_1), i.e., $\frac{1}{2} (A + I_1)$, other than the common-defined term. For example, the CB edge position of pure BiVO₄ can be expressed empirically by [44, 45]

$$E_c = \chi - 1/2E_g + E^e \quad (2)$$

$$= (\chi_{\text{Bi}}^4 \chi_{\text{V}}^4 \chi_{\text{O}}^8)^{1/6} - 1/2E_g + E^e$$

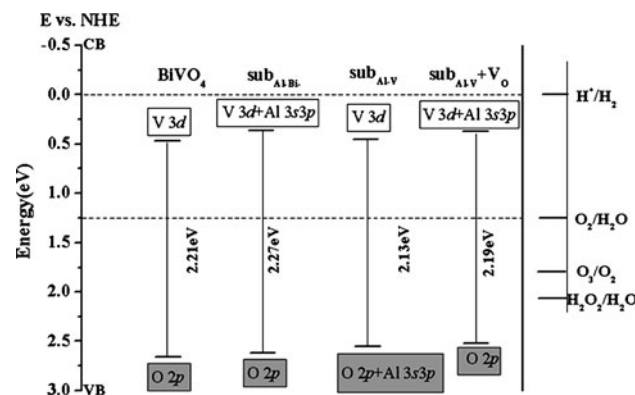
where E_c is the CB edge potential with respect to the normal hydrogen electrode (NHE), E_g is the band gap of the semiconductor, E^e is the energy of free electron on the hydrogen scale (−4.5 eV), and χ is the electronegativity of the semiconductor, which is the geometric mean of the electronegativity of the component atoms. The calculated results are summarized in Table 3.

In order to compare more clearly, the calculated positions of top of valence band (E_{VB}) and bottom of conduction band (E_{CB}) for various defect models are shown in Fig. 6. The results clearly show that the VBM and CBM of *m*BiVO₄ (sub_{Al-Bi}) are raised from those of pure *m*BiVO₄ by about 0.03 and 0.09 eV, respectively. The raising of the CBM suggests that *m*BiVO₄ (sub_{Al-Bi}) would have stronger ability to reduce H⁺ to H₂ than does pure *m*BiVO₄. For

Table 3 Electronegativity and band edge position of various defect models

Models	χ	E_g	E_{CB}	E_{VB}
Pure	6.04	2.21	0.44	2.65
Sub _{Al-Bi}	5.98	2.27	0.35	2.61
Sub _{Al-V}	6.01	2.13	0.45	2.58
Sub _{Al-V} + V _O	5.95	2.19	0.36	2.55

Unit is eV

**Fig. 6** Comparison of the calculated VBM and CBM positions of sub_{Al-Bi}, sub_{Al-V}, and sub_{Al-V} + V_O with respect to NHE scale

mBiVO₄ (sub_{Al-V}), the VBM is raised by about 0.10 eV, so *mBiVO₄* (sub_{Al-V}) should have a reduce ability for oxidation. The CBM is slightly lowered by about 0.01 eV relative to the corresponding values of pure *mBiVO₄*, so *mBiVO₄* (sub_{Al-V}) should have the similar reduction ability. On the contrary, the CBM of *mBiVO₄* (sub_{Al-V} + V_O) is raised by about 0.08 eV, so *mBiVO₄* (sub_{Al-Bi}) and *mBiVO₄* (sub_{Al-V} + V_O) both have the similar ability to reduce H⁺ to H₂. It is well known that H₂O₂ and O₃ can oxidize many organics because of their strong oxidation power, 1.77 eV (H₂O₂) and 2.07 eV (O₃). Compared with them, the three defect models still possess stronger oxidation power. Moreover, sub_{Al-Bi} and sub_{Al-V} + V_O would have stronger ability of photocatalytic water splitting and H₂ evolution than pure *mBiVO₄*.

4 Conclusion

In summary, we calculated the structural and electronic properties of three possible structures to include Al atom into the *mBiVO₄* lattice based on DFT. The optimized geometries indicated that it is more favorable to substitute Al for V site than for Bi site, while the calculated formation energies suggested the substitution of Al for V involving an oxygen vacancy (sub_{Al-V} + V_O) is the energetically most favorable to realize in experiment. The band structures

revealed that an obvious band gap narrowing are observed in sub_{Al-V} and sub_{Al-V} + V_O structures. The most obvious difference is the new state is not appear above the top of VB of the sub_{Al-V} + V_O structure as opposed to the situation in sub_{Al-V} structure in which isolated states are introduced into the band gap. On the other hand, the band gap of *mBiVO₄* (sub_{Al-Bi}) is larger than the measured value of pure *mBiVO₄*. However, the value is still small, so that *mBiVO₄* (sub_{Al-Bi}) should still show well absorption for visible light. Moreover, the density of states analysis showed that both the CBM position of sub_{Al-Bi} and sub_{Al-V} + V_O structures shift upward, which predicts *mBiVO₄* (sub_{Al-Bi} and sub_{Al-V} + V_O) should have a stronger reduction power. The calculated band edge positions demonstrated that the two defect structures have stronger reduction power than pure BiVO₄, while *mBiVO₄* (sub_{Al-V}) structure is without this characteristic. According to the results mentioned above, we can predict theoretically both *mBiVO₄* (sub_{Al-Bi}) and *mBiVO₄* (sub_{Al-V} + V_O) would have stronger ability of photocatalytic water splitting and H₂ evolution than does pure *mBiVO₄*.

Acknowledgments This work was supported by the NSF of China (Grant 20773024), Education Foundation of Fujian Province (NO. JA09015), and the programs for New Century Excellent Talents in University of Fujian Province (HX2006-97).

References

- Errandonea D, Manjon FJ (2008) Prog Mater Sci 53:711
- Tang J, Zou Z, Ye J (2004) Angew Chem Int Ed 43:4463
- Zou Z, Arakawa H (2003) J Photochem Photobiol A Chem 158:145
- Fu H, Zhang L, Yao W, Zhu Y (2006) Appl Catal B Environ 66:10
- Kudo A, Omori K, Kato H (1999) J Am Chem Soc 121:11459
- Tokunaga S, Kato H, Kudo A (2001) Chem Mater 13:4624
- Luo H, Mueller AH, McCleskey TM, Burrell AK, Bauer E, Jia QX (2008) J Phys Chem C 112:6099
- Walsh A, Yan Y, Huda MN, Al-Jassim MM, Wei SH (2009) Chem Mater 21:547
- Chatchai P, Murakami Y, Kishioka S, Nosaka AY, Nosaka Y (2009) Electrochim Acta 54:1147
- Xie BP, Zhang HX, Cai PX, Qiu RL, Xiong Y (2006) Chemosphere 63:956
- Kudo A (2006) Int J Hydrogen Energy 31:197
- Xie B, Zhang H, Cai P, Qiu R, Xiong Y (2006) Chemosphere 63:956
- Xu H, Li H, Wu C, Chu J, Yan Y, Shu H (2008) Mater Sci Eng B 147:52
- Guillodo M, Fouletier J, Dessemont L, Gallo PD (2001) J Eur Ceram Soc 21:2331
- Long M, Cai W, Cai J, Zhou B, Chai X, Wu Y (2006) J Phys Chem B 110:20211
- Xu H, Li H, Wu C, Chu J, Yan Y, Shu H, Gu Z (2008) J Hazard Mater 153:877
- Jiang HQ, Endo H, Natori H, Nagai M, Kobayashi K (2009) Mater Res Bull 44:700
- Ge L (2008) Mater Chem Phys 107:465

19. Ge L (2008) Mater Lett 62:926
20. Yang YL, Qiu L, Harrison WTA, Christoffersen R, Jacobson AJ (1997) J Mater Chem 7:243
21. Kohtani S, Tomohiro M, Tokumura K, Nakagaki R (2005) Appl Catal B Environ 58:265
22. Sayama K, Nomura A, Arai T, Sugita T, Abe R, Yanagida M, Oi T, Iwasaki Y, Abe Y, Sugihara H (2006) J Phys Chem B 110:11352
23. Zhang X, Zhang Y, Quan X, Chen S (2009) J Hazard Mater 167:911
24. Neves MC, Lehocky M, Soares R, Lapcik L, Trindade T (2003) Dyes Pigm 59:181
25. Chatchai P, Murakami Y, Kishioka S, Nosaka AY, Nosaka Y (2009) Electrochim Acta 54:1147
26. Yao W, Iwai H, Ye J (2008) Dalton Trans 11:1426
27. Jiang H, Nagai M, Kobayashi K (2009) J Alloy Compd 24:821
28. Li L, Yan B (2008) J Alloy Compd 476:624
29. Li C, Shi L, Xie D, Du H (2006) J Non-Cryst Solids 352:4128
30. Nie DP, Xue T, Zhang Y, li XJ (2008) Sci China Ser B: Chem 51:823
31. Shon HK, Cho DL, Na SH, Kim JB, Park HJ, Kim JH (2009) J Ind Eng Chem 15:476
32. Li YX, Chen G, Zhang HJ, Li ZH (2009) J Phy Chem Solids 70:536
33. Shirley R, Kraft M (2010) phys Rev B 81:75111
34. Cox DE, Moodenbaugh AR, Sleight AW, Chen HY (1980) NBS Spec Pub 567:189
35. Milman V, Winkler B, White JA, Pickard CJ, Payne MC, Akhmatkaya EV, Nobes RH (2000) Int J Quant Chem 77:895
36. Perdew JP, Chevary JA, Vosko SH, Jackson KA, Pederson MR, Singh DJ, Fiolhais C (1992) Phys Re B 46:6671
37. Perdew JP, Wang Y (1986) Phys Rev B 33:8800
38. Stoltzfus MW, Woodward PM, Seshadri R, Klepeis JH, Bursten B (2007) Inorg Chem 46:3839
39. Nethercot AH (1974) Phys Rev Lett 33:1088
40. Lacomba-Perales R (2008) EPL 83:37002
41. Zhang Y, Holzwarth NAW, Williams RT (1998) Phys Rev B 57:12738
42. Butler MA, Ginley DS (1978) J Electrochem Soc 125:228
43. Zhang SB, Northrup JE (1991) Phys Rev Lett 67:2339
44. Kim Y, Atherton SJ, Brigham ES, Mallouk TE (1993) J Phys Chem 97:11802
45. Parr RG, Pearson RG (1983) J Am Chem Soc 105:7512